Short Papers

Remote Manipulation With a Stationary Computer-Controlled Magnetic Dipole Source

Andrew J. Petruska, Arthur W. Mahoney, and Jake J. Abbott

***Abstract*—In this paper, we examine several magnetic control methods that utilize the fully controllable dipole field generated by the single stationary dipole source. Since the magnetic field generated by a dipole source is nonuniform, it applies both forces and torques to magnetic objects and can be used to manipulate magnetic tools. Recently, the Omnimagnet, a computer-controlled magnetic dipole source capable of varying both its dipole-moment direction and magnitude, was developed to perform magnetic manipulation. The equations and methods are developed generally; therefore, they can be applied to any omnidirectional dipole source, but their effectiveness is demonstrated using the Omnimagnet.**

***Index Terms*—Magnetic manipulation, medical robotics, microrobotics, omnimagnet, teleoperation.**

I. Introduction

Manipulation systems typically require a mechanical connection between the tool and the actuation system to achieve a desired force or torque transfer. This connection is a limiting factor when controlling objects in areas with access restrictions such as minimally invasive surgery, in environments with imaging limitations where a mechanical connection can obscure the field of view, and in low-Reynolds-number fluid environments where a mechanical connection can result in significant environmental disturbances. Using combinations of electromagnets and permanent magnets, a controllable torque and force can be applied to a tool without having a mechanical connection. Fundamentally, there have been two design approaches for electromagnet systems in the past: engineer a field that is aligned in a desired direction with a controllable gradient in the same direction (e.g., MRI systems and Helmholtz with Maxwell coils [1]–[4]) or design a system that has a nonuniform field shape and then calibrate a model or look-up table for the system *in situ* [5]–[12]. Permanent-magnet-based systems have been designed to use follow-the-leader dragging and rotating control approaches, and they have demonstrated dexterous manipulation using the dipole-field model without calibration [8], [9], [13]–[16].

This paper explores the capabilities and limitations of performing magnetic manipulation with an omnidirectional dipole source using the dipole-field equations recently exploited for permanent-magnetic control. Many devices can be modeled as an omnidirectional dipole source at large distances (see, e.g., [5]). Recently, the authors designed the Omnimagnet, which is an omnidirectional electromagnetic source accurately modeled by a point-dipole field comprising three solenoids with a spherical ferromagnetic core nested such that they share the same magnetic center [17]. The analysis in this paper is developed in a general framework allowing for multiple solenoids and non-Omnimagnet-specific equations, but all demonstrations will be performed with an Omnimagnet.

In this paper, we will use bold font to represent vectors (e.g., $\mathbf{a}$, $\mathbf{A}$) and capitalized blackboard font to represent matrices (e.g., $\mathbb{B}$). The two-norm of a vector will be expressed as $\|\mathbf{a}\|$, the inner product of two vectors will be expressed as $\mathbf{a}\cdot\mathbf{b}$, the cross product of two vectors will either be expressed as $\mathbf{a}\times\mathbf{b}$ or in the skew-symmetric matrix form $\mathbb{S}(\mathbf{a})\mathbf{b}$, the unit-length direction of a vector will be written as $\hat{\mathbf{a}}$, and the transpose of a vector or matrix will be expressed as $\mathbf{a}^{\mathrm{T}}$.

II. Magnetics Background

The magnetic field produced by a collection of electromagnets can be modeled with a series expansion, which is called a multipole expansion, if the region of interest is outside of the smallest sphere that encapsulates all of the magnetic sources (i.e., the bounding sphere). The first term in the multipole expansion is called the dipole field, and its magnitude decays with $\|\mathbf{p}\|^{-3}$, where $\mathbf{p}$ is the vector that points from the center of the bounding sphere to the point of interest. The second term, which is called the quadrupole term, decays as $\|\mathbf{p}\|^{-5}$, and the higher order terms decay with monotonically increasing odd powers. By using the multipole expansion, it is possible to have an accurate representation of the magnetic field at distances far from the source (i.e., greater than 1.5 bounding-sphere radii) without having to use computationally intensive (e.g., numerical integration) or experimentally intensive (e.g., *in situ* calibration) techniques [18].

The dipole moment $\mathbf{m}$ of an electromagnetic source when all integral ferromagnetic materials are unsaturated can be written as

$$\mathbf{m} = \mathbb{M}\mathbf{I} \tag{1}$$

where $\mathbb{M}$ is a linear mapping of a column-vector packing of the applied currents $\mathbf{I}$ to the resulting dipole moment $\mathbf{m}$; the rank of $\mathbb{M}$ must be three for magnetic omnidirectionality. The dipole field at any point $\mathbf{p}$, which is relative to the center of the source's bounding sphere, is given by the dipole-field equation:

$$\mathbf{B} = \frac{\mu_0}{4\pi\|\mathbf{p}\|^3}\left(3\hat{\mathbf{p}}\hat{\mathbf{p}}^{\mathrm{T}} - \mathbb{I}\right)\mathbf{m} \tag{2}$$

where $\mathbb{I}$ is a 3×3 identity matrix, and μ_0 is the magnetic permeability of free space [19].

This paper will focus on the manipulation of objects (or tools) that are well modeled by a dipole field, that is, objects that are several bounding-sphere radii away from the source. The tool's dipole moment will be represented as $\mathbf{m}_t$, and, in general, the force $\mathbf{F}$ and torque $\boldsymbol{\mathcal{T}}$ acting on this object when placed in a magnetic field $\mathbf{B}$ are given by [19]

$$\mathbf{F} = (\mathbf{m}_t\cdot\boldsymbol{\nabla})\,\mathbf{B} \tag{3}$$

$$\boldsymbol{\mathcal{T}} = \mathbf{m}_t\times\mathbf{B} \tag{4}$$

where $\boldsymbol{\nabla}$ is the gradient operator.

III. Field Control

Sensing Requirements: Position $\mathbf{p}$.

Limitations: If the desired field is changed rapidly, the system dynamics may not be able to keep up.

Manuscript received November 18, 2013; accepted February 12, 2014. Date of publication August 5, 2014; date of current version September 30, 2014. This paper was recommended for publication by Associate Editor S. Régnier and Editor B. J. Nelson upon evaluation of the reviewers' comments. This work was supported by the National Science Foundation under Grant 0952718 and Grant 0654414.

A. J. Petruska and J. J. Abbott are with the Department of Mechanical Engineering, University of Utah, Salt Lake City, UT 84112 USA (e-mail: Andrew.Petruska@utah.edu; jake.abbott@utah.edu).

A. W. Mahoney is with the School of Computing, University of Utah, Salt Lake City, UT 84112 USA (e-mail: art.mahoney@utah.edu).

Color versions of one or more of the figures in this paper are available online at http://ieeexplore.ieee.org.

Digital Object Identifier 10.1109/TRO.2014.2340111

To determine the dipole moment $\mathbf{m}$ required by the source to produce a desired field $\mathbf{B}$ at some point $\mathbf{p}$, the vector dipole equation (2) must be inverted. Using the dipole field analysis in [15] and [19], it can be shown that the inverse exists of the form

$$\mathbf{m} = \frac{2\pi}{\mu_0}\|\mathbf{p}\|^3 \left(3\hat{\mathbf{p}}\hat{\mathbf{p}}^{\mathrm{T}} - 2\mathbb{I}\right)\mathbf{B}. \tag{5}$$

Combining with (1), the currents required to generate a field are thus

$$\mathbf{I} = \frac{2\pi}{\mu_0}\|\mathbf{p}\|^3 \mathbb{M}^{\dagger}\left(3\hat{\mathbf{p}}\hat{\mathbf{p}}^{\mathrm{T}} - 2\mathbb{I}\right)\mathbf{B} \tag{6}$$

where † identifies a generalized inverse, as $\mathbb{M}$ may not be square, and multiple solutions could exist.

When placed in a magnetic field, an unconstrained magnetic tool will align with the applied field because of the magnetic torque (4) experienced. If the field is rotating, the tool will attempt to keep up with the rotation as well. This tendency to align with the field has been explored using a rotating permanent magnet to propel a ball and helical screw [15]. To perform similar control tasks with a dipole source, the desired field $\mathbf{B}$ in (6) should be rotated at a desired angular velocity $\boldsymbol{\omega}$, and the position should be updated with the tool position. By doing so, a rotating field that translates with the object will be produced and can be used for propulsion. The maximum achievable tool rotation speed $\|\boldsymbol{\omega}_{\max}\|$ is limited by the maximum magnetic torque that can be achieved to counteract the drag torques. The maximum torque, from inspection of (4), is $\|\mathbf{m}_t\|\|\mathbf{B}\|$ and corresponds to the configuration where the tool's dipole moment is consistently orthogonal to the applied rotating field. Operating at a faster speed than this, without increasing the applied field strength, will cause the system to experience step out [1].

A rotating magnetic field generated by an Omnimagnet was used to propel a threaded capsule-endoscope mockup down a transparent lumen in [17]. In that demonstration, helical propulsion through a lumen presented a convenient system for using rotating fields to propel an object because a lumen provides significant physical constraints on the tool's motion. However, these physical constraints are not required to propel an object using a rotating field. To explore using an Omnimagnet for control of adjacent objects in a less constrained environment, a magnetic ball was driven on a flat surface using only position information and a rotating field. The position information was obtained with a vision system, and the drive currents were updated at 100 Hz. The results of driving the ball around a rectangular path on a tabletop and around a Labyrinth maze, shown, respectively, in Fig. 1(a) and (b), demonstrate the capability of the Omnimagnet to control the strength and direction of a field at an arbitrary location in space. Unfortunately, it is possible for disturbances, such as attractive magnetic forces or surface roughness, to apply torques about the dipole moment that cannot be compensated magnetically. In the demonstrations, these disturbances cause the magnet to deviate from a straight trajectory.

Micromanipulation of objects using magnetic torque and force has been explored using multiple-magnet systems that surround the viewing workspace [20]–[22]. The Omnimagnet can produce similar control of microbeads through rolling as demonstrated previously; however, the problem is greatly simplified. Since the micromanipulation workspace is constrained to be under a microscope for viewing, the workspace is necessarily small compared with the Omnimagnet's workspace. As such, the position of the microdevice being manipulated can be assumed to be constant, and a rotating field can be applied in an open-loop fashion. Fig. 1(c) shows the manipulation of a 1-mm magnetic ball in a viscous medium. Using a Reynolds-number analysis, the 1-mm-diameter permanent-magnet sphere in corn syrup (2500 cP, 1.36 g $\cdot$ ml^{-1}) has a behavior equivalent to a 30-μm sphere in water. Note that the Omnimagnet is offset from the workspace by a relatively large distance (150 mm), allowing for manipulation under a microscope with the Omnimagnet placed as necessary to accommodate other equipment.

IV. Torque Control

Sensing Requirements: Position $\mathbf{p}$ and tool dipole moment $\mathbf{m}_t$.

Limitations: Torque can only be applied orthogonal to the tool's dipole moment.

If both the heading and position of the tool are known, it is possible to directly apply a torque. Because of the cross product in (4), no component of torque can be applied parallel to the dipole moment of the tool, reducing the space of achievable torques to those orthogonal to the tool's dipole moment. Thus, it is assumed that any desired torque $\boldsymbol{\mathcal{T}}$ lies in this reachable plane. For any $\boldsymbol{\mathcal{T}}$, there is a 1-D subspace of solutions, parameterized by θ, for the required field and currents

$$\mathbf{B} = \frac{\|\boldsymbol{\mathcal{T}}\|}{\|\mathbf{m}_t\|}(\cot(\theta)\hat{\mathbf{m}}_t + \hat{\boldsymbol{\mathcal{T}}} \times \hat{\mathbf{m}}_t) \tag{7}$$

$$\mathbf{I} = \frac{2\pi\|\boldsymbol{\mathcal{T}}\|\|\mathbf{p}\|^3}{\mu_0\|\mathbf{m}_t\|}\mathbb{M}^{\dagger}(3\hat{\mathbf{p}}\hat{\mathbf{p}}^{\mathrm{T}} - 2\mathbb{I})(\cot(\theta)\hat{\mathbf{m}}_t + \hat{\boldsymbol{\mathcal{T}}} \times \hat{\mathbf{m}}_t). \tag{8}$$

The solution that corresponds to $\theta = \pi/2$ is the minimum-field solution. It represents the case where the applied field is perpendicular to the tool's dipole moment and has been shown to minimize the attractive force between the two dipoles [23].

In some configurations, it is possible to choose a solution that requires less electrical power than the one corresponding to the minimum-field solution and produce the same torque by allowing some field magnitude in the tool's dipole-moment direction and exerting additional force. Letting $\mathbb{R}$ be the positive-definite diagonal matrix packing of the electrical resistance associated with each current, the electrical power required is $\mathbf{I}^{\mathrm{T}}\mathbb{R}\mathbf{I}$. The currents required to produce a torque with minimum electrical power are

$$\mathbf{I} = \frac{4\pi\|\mathbf{p}\|^3}{\mu_0}\mathbb{R}^{-1/2}(\mathbb{S}(\mathbf{m}_t)\left(3\hat{\mathbf{p}}\hat{\mathbf{p}}^{\mathrm{T}} - \mathbb{I}\right)\mathbb{M}\mathbb{R}^{-1/2})^{\dagger}\boldsymbol{\mathcal{T}} \tag{9}$$

where † in this solution is the Moore–Penrose generalized inverse. Alternatively, the unused degree of freedom (DOF) can be used to optimize other favorable parameters, such as minimizing the difference between the resulting force applied and some desired force or direction of motion.

V. Force Control

Sensing Requirements: Position $\mathbf{p}$ and tool dipole moment $\mathbf{m}_t$.

Limitations: A singularity exists when the tool's dipole moment is orthogonal to the position vector, reducing the space of achievable forces in this configuration to the plane spanned by the tool's dipole moment and the position vector.

To apply a controlled force for pushing and pulling tasks, the field gradient at the position of the tool must be controlled. The force between two magnetic dipoles can be expressed as [19]

$$\mathbf{F} = \frac{3\mu_0}{4\pi\|\mathbf{p}\|^4}\mathbb{F}\mathbf{m}$$

$$\mathbb{F} \equiv \mathbf{m}_t\hat{\mathbf{p}}^{\mathrm{T}} + \hat{\mathbf{p}}\mathbf{m}_t^{\mathrm{T}} + (\hat{\mathbf{p}} \cdot \mathbf{m}_t)\,(\mathbb{I} - 5\hat{\mathbf{p}}\hat{\mathbf{p}}^{\mathrm{T}}). \tag{10}$$

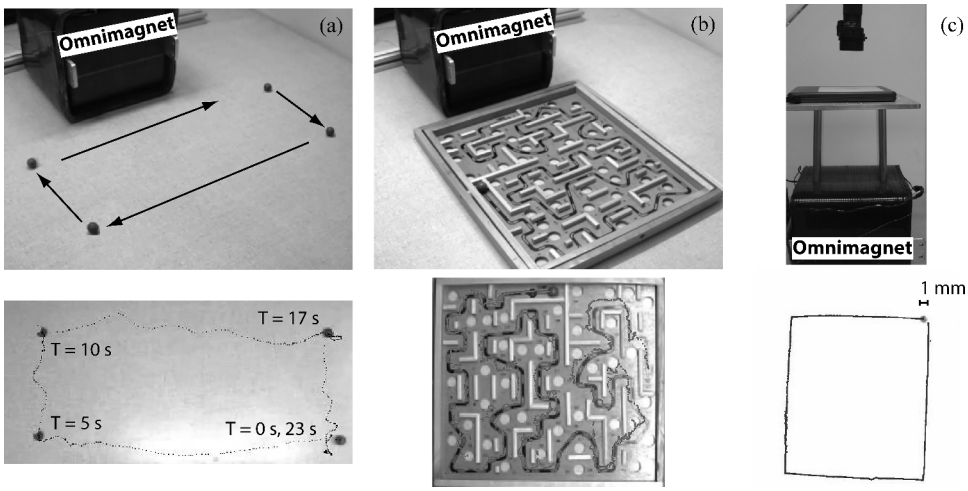

Fig. 1. Position control of a spherical magnet using a rotating field to direct the rolling direction of the ball. (a) 12.5-mm-diameter ball rolling without constraint on a plane adjacent to the Omnimagnet. (b) 12.5-mm diameter ball being directed through a Labyrinth maze adjacent to the Omnimagnet. (c) 1-mm diameter ball rolling in corn syrup on a plane above the Omnimagnet. In (a) and (b), the ball's position is found using computer vision and used in closed-loop control. In (c), the ball is controlled open loop under the assumption that it is always located in the center of the workspace.

Thus, the currents required to apply a particular force $\mathbf{F}$ are

$$\mathbf{I} = \frac{4\pi}{3\mu_0}\|\mathbf{p}\|^4 \mathbb{M}^\dagger \mathbb{F}^{-1}\mathbf{F} \tag{11}$$

$$\mathbb{F}^{-1} = \frac{(2(\hat{\mathbf{p}}\cdot\mathbf{m}_t)^2 + \mathbf{m}_t\cdot\mathbf{m}_t)\mathbb{I} - \mathbb{F}^2}{(\hat{\mathbf{p}}\cdot\mathbf{m}_t)\left((\hat{\mathbf{p}}\cdot\mathbf{m}_t)^2 + \mathbf{m}_t\cdot\mathbf{m}_t\right)}.$$

The inverse of $\mathbb{F}$ exists when the inner product of the tool's dipole moment $\mathbf{m}_t$ and the displacement direction $\hat{\mathbf{p}}$ is nonzero.

When $\mathbf{m}_t$ and $\hat{\mathbf{p}}$ are orthogonal, $\mathbb{F}$ is singular, but forces can still be produced in the plane spanned by $\mathbf{m}_t$ and $\hat{\mathbf{p}}$, and the currents necessary to command a desired force in this plane are

$$\mathbf{I} = \frac{4\pi\|\mathbf{p}\|^4}{3\mu_0\|\mathbf{m}_t\|}\mathbb{M}^\dagger\left(\hat{\mathbf{m}}_t\hat{\mathbf{p}}^{\mathrm{T}} + \hat{\mathbf{p}}\hat{\mathbf{m}}_t^{\mathrm{T}}\right)\mathbf{F}. \tag{12}$$

In the singular configuration, any currents that contribute to a dipole moment not in the span of $\{\mathbf{m}_t, \hat{\mathbf{p}}\}$ create no force. The torque associated with a desired force in the singular configuration is

$$\boldsymbol{\mathcal{T}} = 2\,(\mathbf{m}_t\cdot\mathbf{F})\,\|\mathbf{p}\|(\hat{\mathbf{m}}_t\times\hat{\mathbf{p}}). \tag{13}$$

Therefore, it is possible to apply a torque or a force that would rotate or move the tool such that $\mathbf{m}_t$ is no longer orthogonal to $\hat{\mathbf{p}}$, thereby restoring full force control. Since the direction of the field and the torque applied are not controlled, the resulting force solution will likely be locally rotationally unstable. Consequently, open-loop unconstrained force control with a single dipole source is not feasible in practice. However, if the tool's dipole moment is known, through sensing or mechanical support (e.g., a lumen), pushing and pulling an object using a dipole source with feedback is possible provided the singularity is avoided or appropriately mitigated.

To demonstrate this capability, an axially magnetized permanent magnet disk is fixed to a larger plastic disk, placed in a tub of water, and driven around a rectangular path (see Fig. 2). The buoyant forces on the plastic disk serve to constrain the tool's dipole moment to the vertical direction, and its location is tracked with a vision system. A closed-loop proportional-derivative position controller is used to determine the forces to apply, and (11) is used to convert these into the required electrical currents.

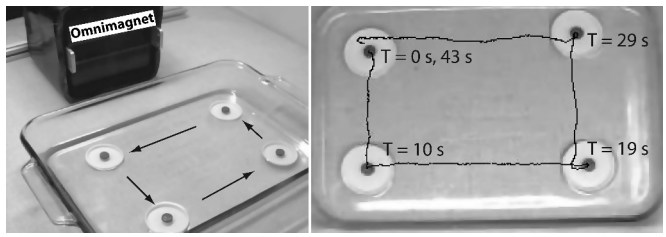

Fig. 2. Position servo control of a floating magnet using applied force, generated by an Omnimagnet [17]. The dipole moment of the magnet is constrained by buoyant forces to be in the vertical direction.

VI. Field-Aligned Force Control

Sensing Requirements: Position $\mathbf{p}$ and tool dipole magnitude $\|\mathbf{m}_t\|$.
Additional Assumptions: The tool is aligned with the applied field.
Limitations: No repulsive forces can be applied to the tool, requiring nonmagnetic forces for system stability. The space of achievable magnetic forces is reduced to a 28° cone opening toward the dipole source. Rapid changes in force direction, relative to the tool's rotational time constant, will cause the tool to become misaligned with the field and the applied force to deviate from the desired force.

Field alignment of an unconstrained tool has been exploited previously for 5-DOF heading and force control [7], [16]. Although it is not possible to achieve 5-DOF control with a single stationary dipole source, 3-DOF force control can be achieved. The force applied to an adjacent magnetic tool from a dipole source when the tool is aligned with the source's field is

$$\mathbf{F} = \frac{3\mu_0\|\mathbf{m}_t\|}{4\pi\|\mathbf{p}\|^4}\frac{((\hat{\mathbf{p}}\cdot\hat{\mathbf{m}})\,\mathbf{m} - (4(\hat{\mathbf{p}}\cdot\hat{\mathbf{m}})^2+1)\|\mathbf{m}\|\hat{\mathbf{p}})}{\sqrt{3(\hat{\mathbf{p}}\cdot\hat{\mathbf{m}})^2+1}}. \tag{14}$$

If a ball with a large magnetic susceptibility were used instead of a permanent magnet, then $\|\mathbf{m}_t\|$ would be a function of the applied field

$$\|\mathbf{m}_t\| = \frac{3\mathcal{V}_b\|\mathbf{m}\|}{4\pi\|\mathbf{p}\|^3}\sqrt{3\,(\hat{\mathbf{p}}\cdot\hat{\mathbf{m}})^2+1} \tag{15}$$

where $\mathcal{V}_b$ is the volume of the unsaturated magnetized ball.

Inspection of (14) shows that the force will always be attractive (i.e., there will always be a component in the $-\hat{\mathbf{p}}$ direction); thus, it is necessary to have an external restoring force (e.g., gravity) to stabilize the direction of attraction. By using the projections $\mathbf{F}\cdot\hat{\mathbf{p}}$ and $\mathbf{F}\cdot\mathbf{F}$, it is possible to obtain a closed-form solution for the required dipole-moment to achieve a desired force

$$\mathbf{m} = \pm\frac{4\pi\|\mathbf{p}\|^4}{3\mu_0\|\mathbf{m}_t\|}\sqrt{\frac{3\left(\hat{\mathbf{p}}\cdot\hat{\mathbf{m}}\right)^2+1}{\left(\hat{\mathbf{p}}\cdot\hat{\mathbf{m}}\right)^2}}\cdot \left(\mathbb{I}-\left(\frac{4\left(\hat{\mathbf{p}}\cdot\hat{\mathbf{m}}\right)^2+1}{3\left(\hat{\mathbf{p}}\cdot\hat{\mathbf{m}}\right)^2+1}\right)\hat{\mathbf{p}}\hat{\mathbf{p}}^{\mathrm{T}}\right)\mathbf{F} \tag{16}$$

where $\left(\hat{\mathbf{p}}\cdot\hat{\mathbf{m}}\right)^2$ is given by

$$\left(\hat{\mathbf{p}}\cdot\hat{\mathbf{m}}\right)^2 = \frac{7\left(\hat{\mathbf{F}}\cdot\hat{\mathbf{p}}\right)^2-6\pm\left(\hat{\mathbf{F}}\cdot\hat{\mathbf{p}}\right)\sqrt{17\left(\hat{\mathbf{F}}\cdot\hat{\mathbf{p}}\right)^2-16}}{18-16\left(\hat{\mathbf{F}}\cdot\hat{\mathbf{p}}\right)^2}. \tag{17}$$

The magnitude of $\mathbf{m}$ is always

$$\|\mathbf{m}\| = \frac{4\pi\|\mathbf{p}\|^4}{3\mu_0\|\mathbf{m}_t\|}\frac{-\left(\mathbf{F}\cdot\hat{\mathbf{p}}\right)}{\sqrt{3\left(\hat{\mathbf{p}}\cdot\hat{\mathbf{m}}\right)^2+1}}. \tag{18}$$

When a solution exists, (16) provides four choices of $\mathbf{m}$ that will apply the same force—two directions, each in the positive or negative sense. In the special case when $\hat{\mathbf{F}}\cdot\hat{\mathbf{p}}=1$, one solution for $\hat{\mathbf{p}}\cdot\hat{\mathbf{m}}$ is 0 corresponding to the force singularity. In this configuration, (16) no longer yields a solution for the dipole moment; however, there exists an infinite number of solutions corresponding to dipole moments in the plane defined by $\hat{\mathbf{p}}\cdot\hat{\mathbf{m}}=0$ with a magnitude given by (18).

Together, (17) and (18) define a geometric constraint on what force directions can be achieved when the tool is aligned with the dipole field:

$$\hat{\mathbf{F}}\cdot\hat{\mathbf{p}} \le -\sqrt{\frac{16}{17}}. \tag{19}$$

This constraint requires any applied force to be attractive (i.e., have a component in the $-\hat{\mathbf{p}}$ direction), and confines an applied force direction to differ from the $\hat{\mathbf{p}}$ direction by no more than $\arccos\left(\sqrt{16/17}\right)\approx 14^\circ$, and, thus, constrains the workspace of the tool to a 28° cone emanating from the center of the dipole source and directed along the direction of the restoring force. Without loss of generality, we will assume for the remainder of this discussion that the restoring force is gravity, that it acts in the $-\hat{\mathbf{z}}$ Cartesian direction, and that the dipole source is located at the origin.

To discuss the manipulability of a tool in this framework, it is useful to switch to a cylindrical coordinate frame where the axis of the cylinder is aligned with the $\hat{\mathbf{z}}$-direction, and the radial and circumferential directions describe motion in a horizontal plane below the dipole source. The location of a tool will be defined by $(z\hat{\mathbf{z}}, r\hat{\mathbf{r}}, \phi\hat{\boldsymbol{\phi}})$, but because of symmetries in the dipole field, only the z and r values will affect the following discussion. In this framework, the angle $\theta=\arctan(r/z)$ will describe where in the conic workspace the tool is operating.

In the achievable workspace, $\hat{\mathbf{p}}$ will always have its largest component in the $-\hat{\mathbf{z}}$-direction (i.e., the restoring force direction), and (19) further requires the largest component of any achievable force to be in the $+\hat{\mathbf{z}}$-direction. Therefore, it is convenient to normalize any applied horizontal force with the applied vertical force with the understanding that as the applied vertical force is reduced to zero, any horizontal components must also go to zero. Fig. 3 shows how the space of achievable radial and circumferential forces changes as the tool moves from being positioned directly under the source ($r=0\Leftrightarrow\theta=0^\circ$) to being positioned at the edge of the conic workspace ($r=z/4\Leftrightarrow\theta\approx 14^\circ$). The manipulability measure in the figure is defined as the minimum horizontal force (which is always in the positive radial direction) normalized by the maximum horizontal force (which is always in the negative radial direction). As the tool moves toward the boundary, the manipulability measure goes to zero because the achievable forces in both the circumferential and the positive radial directions go to zero.

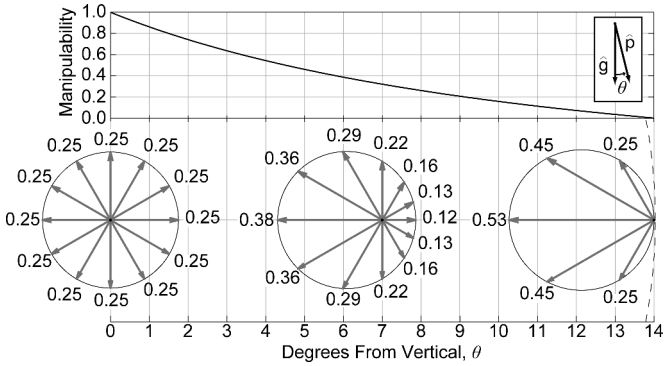

Fig. 3. (Top) Manipulability measure of a tool aligned with a source's dipole field as a function of angular position inside of the 28° conic workspace. The manipulability is the ratio of minimum to maximum force that can be applied to the tool in the horizontal plane by the source. (Bottom) Achievable forces at three locations from the center ($\theta=0^\circ$) to the edge ($\theta=14^\circ$) of the cone. The magnitude of these forces are normalized by the applied vertical force; as the vertical force tends to zero, the horizontal forces must also go to zero. As the tool moves away from vertical alignment ($\theta=0^\circ$), larger forces can be generated to push it toward $\theta=0^\circ$ than to push it toward the edge of the workspace.

Unfortunately, the geometric force constraint (19) prevents general application of (16). To implement a controller with this method, it is necessary to determine the set of achievable forces and then pick an achievable force that yields, as close as possible, the response required by the control system. As before, it is beneficial to split the desired force into a component parallel to the restoring force and one perpendicular to the restoring force: $\mathbf{F}=F_z\hat{\mathbf{z}}+\mathbf{F}_\perp$. For $\mathbf{F}$ to be achievable, F_z must be positive, and $\|\mathbf{F}_\perp\|$ must be small enough to satisfy (19). The maximum achievable $\|\mathbf{F}_\perp\|$ can be found by finding a positive value of α, where

$$\mathbf{F}=F_z\hat{\mathbf{z}}+\alpha\hat{\mathbf{F}}_\perp \tag{20}$$

which satisfies (19) at the constraint boundary. This yields a quadratic equation for α

$$\left((\hat{\mathbf{p}}\cdot\hat{\mathbf{F}}_\perp)^2-\frac{16}{17}\right)\alpha^2+2F_z((\hat{\mathbf{p}}\cdot\hat{\mathbf{z}})(\hat{\mathbf{p}}\cdot\hat{\mathbf{F}}_\perp))\alpha + F_z^2\left((\hat{\mathbf{p}}\cdot\hat{\mathbf{z}})^2-\frac{16}{17}\right)=0. \tag{21}$$

Thus, the dipole moment that should be applied given a desired force and a restoring-force direction requires that $\mathbf{F}$ in (16) and (17) be $F_z\hat{\mathbf{z}}+\min(\|\mathbf{F}_\perp\|,\alpha)\hat{\mathbf{F}}_\perp$, where α is the positive real solution to (21). If a positive and real solution for α exists, and if $\alpha\ge\|\mathbf{F}_\perp\|$, then the desired force can be achieved; otherwise, if $\alpha<\|\mathbf{F}_\perp\|$, then the desired force in the perpendicular direction cannot be achieved and must be reduced to have a magnitude of α. If no positive solution for α exists, then it is not possible to apply a force in the positive $\hat{\mathbf{F}}_\perp$ direction, which happens at the edge of the achievable workspace. If no real solution exists, then it is not possible to achieve $F_z\hat{\mathbf{z}}$ at this location, which happens if the position is outside of the achievable workspace.

A semiboyant capsule was levitated and driven along a rose curve using this field-aligned force control approach, as shown in Fig. 4,

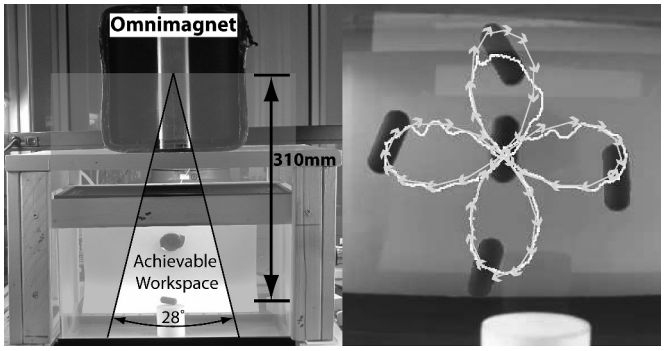

Fig. 4. Semiboyant capsule is levitated and position controlled about a rose curve using a field-aligned force control approach. The achievable workspace is confined to the 28° cone shown.

using a proportional-derivative controller with visual tracking at a 30-Hz update rate. The orientation of the capsule shows the applied field direction required at each snapshot to achieve the control forces. If the manipulated tool were a sphere, the uncontrolled orientation would not be seen. The capsule has larger tracking error closer to the Omnimagnet; this is likely because the assumption that the Omnimagnet's field is a pure dipole field has more error close to the Omnimagnet, with the error reducing with $\|\mathbf{p}\|^{-7}$ [17]. The tracking error could be reduced by moving the trajectory farther from the Omnimagnet.

VII. Comment on Reflective Force and Torque

Because the Omnimagnet used in these demonstrations contains a spherical ferromagnetic core, the permanent magnet used in a magnetic tool will slightly magnetize the core, causing the permanent magnet to be slightly attracted to the Omnimagnet even when no power is applied. Assuming the permanent-magnet tool can be modeled as a point dipole, which is reasonable for relatively large separation distances [18], the dipole moment of the soft-magnetic core, $\mathbf{m}_c$, due to the permanent magnet, $\mathbf{m}_t$, can be determined by the method provided in [17]

$$\mathbf{m}_c = \frac{R_c^3}{\|\mathbf{p}\|^3}\left(3\hat{\mathbf{p}}\hat{\mathbf{p}}^{\mathrm{T}} - \mathbb{I}\right)\mathbf{m}_t \tag{22}$$

where R_c is the radius of the core. The torque and force on the magnetic tool due to the reflection are

$$\boldsymbol{\mathcal{T}} = \frac{3\mu_0 R_c^3}{4\pi\|\mathbf{p}\|^6}(\hat{\mathbf{p}}\cdot\mathbf{m}_t)(\mathbf{m}_t\times\hat{\mathbf{p}}) \tag{23}$$

$$\mathbf{F} = -\frac{3\mu_0 R_c^3\|\mathbf{m}_t\|^2}{4\pi\|\mathbf{p}\|^7}\left(3\hat{\mathbf{m}}_t\hat{\mathbf{m}}_t^{\mathrm{T}} + \mathbb{I}\right)\hat{\mathbf{p}}. \tag{24}$$

For perspective, if a 1-cm^3 NdFeB grade-N52 magnet, which has a dipole moment of 1.17 A $\cdot$ m^2, is placed at the surface of the outer coil of an Omnimagnet with the same geometry as the one used in the experiments, the maximum torque would be 59 $\times 10^{-3}$ mN $\cdot$ m, and the maximum force would be 5.3 mN (only 7% of its weight). To account for this coupling, the Omnimagnet's solenoid currents can be controlled such that the net dipole moment of the Omnimagnet becomes zero by using (1) to calculate the currents required to create a dipole moment that is the negative of (22) and, then, adding that quantity to whatever dipole moment is required for the task. This adjustment was not necessary in the above demonstrations because of the relatively low reflective torques and forces at the operation distances of the demonstrations, and because of the closed-loop controllers used. However, since the reflective torque and force scales with the square of the tool's dipole moment, this effect could become significant for magnetically stronger tools. Although this analysis assumes a spherical core, the scaling will be similar for dipole sources that contain nonspherical ferromagnetic elements.

VIII. Conclusion

A single stationary electromagnetic dipole source can be used to manipulate adjacent tools using several methods. If both the position and heading of the tool are known or sensed, direct force and torque control methods can be applied. If only position information is available, in many instances, it is possible to assume the tool will attempt to align with the applied field, enabling both rotating-field control and field-aligned force control approaches. Unfortunately, the workspace for field-aligned force control is fairly limited. Many demonstrations in this paper are conducted in 2-D workspaces, e.g., ball rolling; however, the methods developed for manipulation with a single controlled source are equally applicable to general 3-D workspaces under the provided assumptions.

References

[1] K. Ishiyama, M. Sendoh, A. Yamazaki, and K. I. Arai, "Swimming micro-machine driven by magnetic torque," *Sens. Actuators A*, vol. 91, pp. 141–144, 2001.

[2] K. B. Yesin, K. Vollmers, and B. J. Nelson, "Modeling and control of untethered biomicrorobots in a fluidic environment using electromagnetic fields," *Int. J. Robot. Res.*, vol. 25, nos. 5/6, pp. 527–536, 2006.

[3] J. B. Mathieu, G. Beaudoin, and S. Martel, "Method of propulsion of a ferromagnetic core in the cardiovascular system through magnetic gradients generated by an MRI system," *IEEE Trans. Biomed. Eng.*, vol. 53, no. 2, pp. 292–299, Feb. 2006.

[4] S. Jeon, G. Jang, H. Choi, and S. Park, "Magnetic navigation system with gradient and uniform saddle coils for the wireless manipulation of micro-robots in human blood vessels," *IEEE Trans. Magn.*, vol. 46, no. 6, pp. 1943–1946, Jun. 2010.

[5] M. Grady, M. Howard III, J. Molloy, R. Ritter, E. Quate, and G. Gillies, "Nonlinear magnetic stereotaxis: Three-dimensional, in vivo remote magnetic manipulation of a small object in canine brain," *Med. Phys.*, vol. 17, pp. 405–415, 1990.

[6] D. Meeker, E. H. Maslen, R. C. Ritter, and F. Creighton, "Optimal realization of arbitrary forces in a magnetic stereotaxis system," *IEEE Trans. Magn.*, vol. 32, no. 2, pp. 320–328, Mar. 1996.

[7] M. P. Kummer, J. J. Abbott, B. E. Kratochvil, R. Borer, A. Sengul, and B. J. Nelson, "OctoMag: An electromagnetic system for 5-DOF wireless micromanipulation," *IEEE Trans. Robot.*, vol. 26, no. 6, pp. 1006–1017, Dec. 2010.

[8] M. H. Hagiwara, T. K. Kawahara, Y. Yamanishi, and F. Arai, "Driving method of microtool by horizontally arranged permanent magnets for single cell manipulation," *Appl. Phys. Lett.*, vol. 97, pp. 013701-1–013701-3, 2010.

[9] G. Ciuti, P. Valdastri, A. Menciassi, and P. Dario, "Robotic magnetic steering and locomotion of capsule endoscope for diagnostic and surgical endoluminal procedures," *Robotica*, vol. 28, no. 2, pp. 199–207, 2010.

[10] M. Mehrtash and M. B. Khamesee, "Design and implementation of LQG\LTR controller for a magnetic telemanipulation system-performance evaluation and energy saving," *Microsyst. Technol.*, vol. 17, no. 5–7, pp. 1135–1143, 2011.

[11] A. Komaee and B. Shapiro, "Steering a ferromagnetic particle by optimal magnetic feedback control," *IEEE Trans. Control Syst. Technol.*, vol. 20, no. 4, pp. 1011–1024, Jul. 2012.

[12] P. Berkelman and M. Dzadovsky, "Magnetic levitation over large translation and rotation ranges in all directions," *IEEE/ASME Trans. Mechatronics*, vol. 18, no. 1, pp. 44–52, Feb. 2013.

[13] M. Simi, G. Sardi, P. Valdastri, A. Menciassi, and P. Dario, "Magnetic levitation camera robot for endoscopic surgery," in *Proc. IEEE Int. Conf. Robot. Autom.*, 2011, pp. 5279–5284.

[14] A. W. Mahoney and J. J. Abbott, "Managing magnetic force applied to a magnetic device by a rotating dipole field," *Appl. Phys. Lett.*, vol. 99, pp. 134103-1–134103-3, 2011.

[15] A. W. Mahoney and J. J. Abbott, "Generating rotating magnetic fields with a single permanent magnet for propulsion of untethered magnetic devices in a lumen," *IEEE Trans. Robot.*, vol. 30, no. 2, pp. 411–420, Apr. 2014.
[16] A. W. Mahoney and J. J. Abbott, "5-DOF manipulation of a magnetic capsule in fluid using a single permanent magnet: Proof-of-concept for stomach endoscopy," in *Proc. Hamlyn Symp. Med. Robot.*, 2013, pp. 114–115.
[17] A. J. Petruska and J. J. Abbott, "Omnimagnet: An omnidirectional electromagnet for controlled dipole-field generation," *IEEE Trans. Magn.*, vol. 50, no. 7, p. 8400810, Jul. 2014.
[18] A. J. Petruska and J. J. Abbott, "Optimal permanent-magnet geometries for dipole field approximation," *IEEE Trans. Magn.*, vol. 49, no. 2, pp. 811–819, Feb. 2013.
[19] D. J. Griffiths, *Introduction to Electrodynamics*. Englewood Cliffs, NJ, USA: Prentice-Hall, 1999.
[20] M. Gauthier and E. Piat, "Control of a particular micro-macro positioning system applied to cell micromanipulation," *IEEE Trans. Autom. Sci. Eng.*, vol. 3, no. 3, pp. 264–271, Jul. 2006.
[21] C. Pawashe, S. Floyd, and M. Sitti, "Modeling and experimental characterization of an untethered magnetic micro-robot," *Int. J. Robot. Res.*, vol. 28, no. 8, pp. 1077–1094, 2009.
[22] L. Zhang, J. Abbott, L. Dong, B. Kratochvil, D. Bell, and B. Nelson, "Artificial bacterial flagella: Fabrication and magnetic control," *Appl. Phys. Lett.*, vol. 94, pp. 064107-1–064107-3, 2009.
[23] A. W. Mahoney, S. E. Wright, and J. J. Abbott, "Managing the attractive magnetic force between an untethered magnetically actuated tool and a rotating permanent magnet," in *Proc. IEEE Int. Conf. Robot. Autom.*, 2013, pp. 5346–5351.

Constraint-Based Prioritized Trajectory Planning for Multibody Systems

Yuichi Tazaki and Tatsuya Suzuki

***Abstract*—This paper presents a trajectory-planning method for multibody systems. Trajectory planning of a multibody system is formulated as a constraint-solving problem on a set of variables expressing the motion of the multibody system over a finite-time interval. Constraints express the dynamics of rigid bodies, kinematic conditions of joints, various range limitations, as well as achievement of tasks, and they can be assigned different priority levels. The prioritized constraint-solving problem is then treated under the framework of lexicographical goal programming, where the local optimality of the problem is characterized in terms of Pareto efficiency condition. Based on this observation, an algorithm that iteratively updates the variables toward a locally optimal solution is derived. The proposed method is evaluated in simulation examples.**

***Index Terms*—Constraint solving, multibody systems, priority, trajectory planning.**

Manuscript received May 26, 2013; revised March 30, 2014; accepted April 19, 2014. Date of publication May 23, 2014; date of current version September 30, 2014. This paper was recommended for publication by Associate Editor N. Mansard and Editor A. Kheddar upon evaluation of the reviewers' comments.

The authors are with the Graduate School of Engineering, Nagoya University, Nagoya 464-8601, Japan (e-mail: tazaki@nuem.nagoya-u.ac.jp; t_suzuki@nuem.nagoya-u.ac.jp).

Color versions of one or more of the figures in this paper are available online at http://ieeexplore.ieee.org

Digital Object Identifier 10.1109/TRO.2014.2320794

I. Introduction

Trajectory planning of robotic systems with many degrees of freedom poses some technical challenges. First, one must find a trajectory that achieves given tasks, while fulfilling kinematic and physical constraints in a high-dimensional state space. Trajectory planning is often treated as an optimization problem (see [1]–[7]). Here, a set of physical variables that express a robotic trajectory is optimized to fulfill a series of constraints that originates from law of physics and various kinematic relationships between objects. A wide range of optimization techniques have been investigated, including the Newton method [3], the shooting method [2], [4], the covariance matrix adaptation [5], and the SQP [7].

The second difficulty is the multiobjective nature that most real-world trajectory planning problems possess. The task-space control framework is capable of handling different priorities of tasks (see [8]–[13]). In this framework, a unique local coordinate frame called a task space is defined for each task and tasks with lower priorities are treated in the null-space of the task spaces of those with higher priorities. This framework is extended to inequality tasks in [14]. Although it is quite useful for synthesizing a set of feedback controllers with multiple priority levels, it is not directly applicable to trajectory planning. When one considers trajectory planning, task priorities should be considered in the space of state trajectories rather than in the space of states. However, trajectory planning is a nonlinear problem in much higher dimension space. This makes some computational techniques that have been used in task-space control not directly applicable. These include the computation of the pseudoinverse matrix of constraint Jacobian (see [8]), the computation of the basis of constraint null-space using singular value decomposition (see [12]), and sequence of quadratic programs (see [14]).

Based on the above background, this paper proposes a trajectory planning method for robotic systems that are represented as multibody systems. The multibody representation enables the expression robots with various morphologies and workspaces with different settings in a uniform manner. A trajectory-planning problem of a multibody system is formulated as a constraint satisfaction problem with multiple priority levels, in which the kinematics and the dynamics of the multibody system, as well as the achievement of tasks are expressed as a set of constraint conditions. It is shown that the problem can be viewed as a class of goal programming problem (see [18]) and its local optimality condition is given as a special form of Pareto-efficiency condition. Based on this observation, an algorithm that iteratively updates a set of decision variables toward a prioritized Pareto-efficient point is proposed. The proposed algorithm requires no expensive computation other than the solution of quadratic programs, and therefore, it is suitable for trajectory planning of robotic systems with many degrees of freedom. The basic concept of the proposed method has been presented in the authors' previous publications (see [16] and [17]). In this paper, the theoretical foundation of the proposed method is strengthened by revealing the connection between lexicographical optimality and a special type of Pareto-efficiency (see Section II). The formulation of multibody trajectory planning is presented considering both sparse and dense parameterizations (see Section III). Moreover, the computational performance of the proposed method is compared with conventional multiobjective optimization problems that are computed by a generic solver (see Section IV). Concluding remarks are made in Section V.

Notation: A sequence of integers from $i_1, i_1+1, \ldots, i_2$ is written as $[i_1 : i_2]$. Moreover, the vertical concatenation of vectors, $[v_1^\mathsf{T}\ v_2^\mathsf{T}]^\mathsf{T}$ is written as $[v_1; v_2]$. For a vector c and an index set $\mathcal{I}$, $c_\mathcal{I}$ denotes the subvector of c with the components indexed by $\mathcal{I}$.